PHYSICAL REVIEW A VOLUME 39, NUMBER 7 APRIL 1, 1989

Quantum fluctuation and correlations in the stimulated Raman scattering spectrum

D. C. MacPherson, R. C. Swanson, and J. L. Carlsten
Physics Department, Montana State University, Bozeman, Montana 59717
(Received 27 October 1988)

Spectral correlations from theoretical and experimental studies of the fluctuations in the single-shot stimulated Raman scattering spectrum are presented. The coherence-mode representation of the Stokes field is demonstrated as a convenient and somewhat intuitive method of generating ensembles of the fields and spectra. The theory is shown to reproduce the observed spectral fluctuations. In addition, other theoretical approaches are shown to be in agreement with coherence-mode theory.

I. INTRODUCTION

Generation of a Stokes radiation pulse from spontaneous emission and its amplification to a large macroscopic field has recently been the subject of considerable research. To treat the spontaneous initiation, Heisenberg equations of motion for the Stokes field operators and Raman medium are coupled to a classical pump field. Fluctuations arise from the statistical nature of the spontaneous emission and from collisional effects. Raymer and Mostowski[1] have presented a fully quantum mechanical derivation of the Heisenberg equations of motion for the Stokes field. The initiating fluctuations can be amplified to obtain large scale fluctuations in the energy, spectrum, and temporal shape of the output pulses. Large energy fluctuations were observed and theoretically modeled for Stokes pulses before pump depletion.[2] Recently dramatic spectral fluctuations were observed after substantial pump depletion.[3] Englund and Bowden[4,5] have shown that on occasional shots, the initiating fluctuations will generate a Stokes field with a near π phase shift which can initiate a soliton pulse to form in the depletion region of the pump pulse.

Similar fluctuations have also been observed in other single-pass gain media such as the single-pass dye laser[6] and in superfluorescence.[7,8] These three systems are all examples of optically pumped, pulsed single-pass lasers. The properties of the light emitted from a pulsed single-pass laser is quite different from that generated in a pulsed recirculating cavity laser. The most obvious difference is in the power spectrum of the emitted radiation.[3,6] In a cavity laser the allowed frequencies are determined by the discrete modes associated with the laser cavity. In a single-pass laser such as a Raman generator, single-pass dye laser, or optically pumped superfluorescence medium there is no cavity to influence the spectrum.

To give a fully quantum mechanical description of the buildup of the laser pulse from spontaneous emission and generate an ensemble of shots, one first chooses a complete set of modes for expanding the radiation field. While the choice of cavity modes is obvious for a recirculating laser, for a single-pass laser the most intuitive choice is not clear. In this paper we review the particularly useful choice of localized coherence modes which were developed earlier.[9] Using this particular set of modes we can make an interesting comparison between the two types of lasers.

In a pulsed recirculating laser one can insert additional etalons in the optical cavity. If the laser pulse stays in the cavity long enough to adequately sample all the frequency selective elements, all but one mode can be suppressed resulting in a near-single-mode output pulse. Using the Raman generator as an example of a single-pass laser and expanding the Stokes field in coherence modes one again finds that if the growing pulse remains in the amplifying medium long enough (thus better sampling the frequency of the Raman transition) the number of significantly excited modes is reduced. For a Raman generator, the number of significantly excited modes can also be varied by changing the Raman linewidth, which depends on the pressure.

Large spectral fluctuations can be observed when the output Stokes pulse has several modes which on average are significantly excited. Although the power spectra of the individual coherence modes are identical for each shot, when the modes are added together with weighted random amplitudes and random phases, the resulting power spectrum has large fluctuations. These spectral fluctuations were recently observed in a Raman generator.[3] While observing the single shot Stokes spectra from a Raman generator it was found that some shots were near transform limited while other shots had a broad spiky spectrum.

It is the purpose of this paper to present theoretical calculations of the Raman spectral fluctuations and compare them with the experimentally measured results. We first describe the coherence mode expansion and how it was used to model the experiment. Next we give the details of how the experiment was done followed by a comparison with theory. In Sec. V we discuss some of the details of pump depletion. Finally two additional methods for theoretically generating Raman spectra are presented which give results similar to those obtained using the coherence-mode approach.

II. THEORY

A fully quantum-mechanical approach to treating the problem of growing a macroscopic field from spontane-

ous emission in a Raman generator using coherence modes has been presented by Raymer *et al.*[2,9] We have applied this approach to our system with the assumption that only a single transverse mode of the Stokes beam is excited. We believe this assumption is valid because the pump beam used was near single transverse mode and because of the multipass cell geometry used to pump the Raman generator.

A. Coherent expansion

Before describing the coherence-mode theory in more detail a few points should be made about the theory. For a given location in the Raman medium the coherence modes are identical for all shots. Therefore the magnitude of the complex degree of coherence[10] has its maximum value of one for the individual modes. Fluctuations occur because of variations in the level of excitation and phase of each mode from shot to shot.

Quantum initiation is included through both a Langevin noise operator associated with collisional damping and by an initial polarization in the medium. The noise operator must be included to maintain operator consistency in the Heisenberg equations of motion.[11] Without the noise operator the expectation value of the number of atoms in the ground state can be shown to decay even in the absence of any interaction. The initial polarization is included because the atomic coherence operator does not commute with the atomic inversion operator. Therefore one cannot specify both that the system starts in the ground state and that the initial polarization is zero. As a possible physical picture, imagine that one measures the polarization of an ensemble of single hydrogen molecules which are prepared in their ground state. Each molecule would have a finite polarization with an average order of magnitude of ea_0. However if the polarization of a sample of hydrogen gas is measured the magnitude of the resulting polarization per atom would be proportional to $\sqrt{N}/N$ due to random orientations. This simple model gives the correct magnitude of the fluctuating polarization which initiates the stimulated emission. Of course the spontaneous emission can alternatively be attributed to a combination of vacuum field fluctuations and polarization fluctuations.[7,12,13]

An appealing feature of using the coherence modes approach is that q-number equations are not replaced with stochastic c-number equations. Instead, the operator equations are used to calculate the two time coherence function which depends only on expectation values of the system and Langevin operators. Once the correlation function is calculated for a given gain and location in the Raman generator it is used to generate the temporal coherence modes. Next a particular realization of the electric field is formed by adding these modes together with random phases and Gaussian amplitude statistics. This can be done many times to generate an ensemble of temporal Stokes pulses. Since this is the last stage of the calculation before depletion it is easy to generate a large ensemble which can be used to calculate statistics.

We will present here the outline and results of the theory. The details are presented in Ref. 9. For the case of no pump depletion and a classical field E_L, the Heisenberg equations of motion for the negative frequency component of the Stokes field operator $\hat{E}_s^{(-)}$ and system polarization operator $\hat{Q}(z,\tau)=|3\rangle\langle 1|\exp[-i(\omega_L-\omega_S)\tau]$ in the retarded frame are[9]

$$\begin{aligned}\frac{\partial \hat{E}_s^{(-)}(z,\tau)}{\partial z}&=-ik_2\hat{Q}^{\dagger}(z,\tau)E_L(z,\tau)\,,\\ \frac{\partial \hat{Q}^{\dagger}(z,\tau)}{\partial \tau}&=-\Gamma\hat{Q}^{\dagger}(z,\tau)+ik_1E_L^{*}(z,\tau)\hat{E}_s^{(-)}(z,\tau)\\ &\quad+\hat{F}^{\dagger}(z,\tau)\,,\end{aligned}\tag{1}$$

where Γ is the collisional dephasing rate and a Langevin driving term $\hat{F}^{\dagger}$ has been added to maintain the operator consistency of $\hat{Q}$. The constants k_1 and k_2 are defined in Ref. 9 but their values will be used as fitting parameters here. The initial condition for $\hat{Q}$ and the correlation for the Langevin operator $\hat{F}$ are

$$\begin{aligned}\langle \hat{Q}^{\dagger}(z,\tau=0)\hat{Q}(z',\tau=0)\rangle&=\rho^{-1}\delta(z-z')\,,\\ \langle \hat{F}^{\dagger}(z,\tau)\hat{F}(z',\tau')\rangle&=(2\Gamma\rho^{-1})\delta(z-z')\delta(\tau-\tau')\,,\end{aligned}\tag{2}$$

where ρ is the linear number density and the expectation value is taken in the ground state. Solving the coupled equations (1) for the Stokes field operator the two-time correlation function for the Stokes field can be calculated. The two time correlation function for a single transverse Stokes mode is defined in terms of the field operators as

$$G(\tau_1,\tau_2)=\frac{c}{2\pi\hbar\omega_s}[\langle \hat{E}_s^{(-)}(z,\tau_1)\hat{E}_s^{(+)}(z,\tau_2)\rangle]\,.\tag{3}$$

Substituting the solution of Eq. (1) with (2) into Eq. (3) the two time correlation function is obtained. We chose to normalize the correlation function so that $G(\tau_c,\tau_c)=1$ where τ_c is the center of the laser temporal pulse, and obtained

$$\begin{aligned}G(\tau_1,\tau_2)=&\frac{E_L(\tau_1)E_L^{*}(\tau_2)}{2|E_L(\tau_c)|^2q(\tau_1,\tau_2)}e^{-\Gamma(\tau_1+\tau_2)}\\ &\times\left\{f(\tau_1,\tau_2)+2\Gamma\int_0^{T}e^{2\Gamma\tau'}g(\tau')d\tau'\right\}\,,\end{aligned}\tag{4a}$$

where

$$\begin{aligned}q(\tau_a,\tau_b)&=4k_1k_2z\int_{\tau_b}^{\tau_a}|E_L(\tau')|^2d\tau'\,,\\ f(\tau_1,\tau_2)&=[q(\tau_1,0)]^{1/2}I_1([q(\tau_1,0)]^{1/2})\\ &\quad\times I_0([q(\tau_2,0)]^{1/2})-(1\leftrightarrow 2)\,,\\ g(\tau')&=[q(\tau_1,\tau')]^{1/2}I_1([q(\tau_1,\tau')]^{1/2})\\ &\quad\times I_0([q(\tau_2,\tau')]^{1/2})-(1\leftrightarrow 2)\,,\end{aligned}\tag{4b}$$

where $(1\leftrightarrow 2)$ indicates interchange of τ_1 and τ_2 and T is the smaller of τ_1 and τ_2. Since the overall amplitude of the correlation function is not of particular interest here, there are only two free parameters to choose once the pump field has been prescribed. These parameters are the gain times the length of the medium ($4k_1k_2z$) and the Raman linewidth (Γ). We will be comparing the theory with an experiment at 32 atmospheres of H_2. Using the

result from measurements by Bishel[14] we obtained a value for Γ of 4.7 Giga rad/sec half width at half maximum (HWHM). Since the temporal pulse shape from our laser is nearly Gaussian and the pulse is single mode was approximated $E_L(\tau)$ by a normalized Gaussian times an amplitude E_0,

$$E_L(\tau)=\frac{E_0}{(\sigma\pi^{1/2})^{1/2}}\exp\left[-\frac{(\tau-\tau_c)^2}{2\sigma^2}\right] . \quad (5)$$

Experimentally the $1/e$ width σ of the temporal intensity is 15 ns giving a FWHM of 26 ns. This leaves the quantity $\beta\equiv 4k_1k_2E_0^2z$ as an adjustable parameter. We determined the value of β by varying it until the calculated average gain narrowed linewidth agreed with that obtained experimentally. In the coherence mode theory the average linewidth is found by evaluating the coherence function at equal times. However experimentally we measured the linewidth after pump depletion and the coherence modes theory is only valid before depletion. If the linewidth does not change significantly through depletion (as we will shown is the case) our method for obtaining β is valid. We found that $\beta=10\,000$ [which corresponds to a normal steady-state (SS) peak gain of $G_{SS}\equiv 4k_1k_2zE_L^2(\tau_c)/2\Gamma=38$] gave good agreement with the experimental linewidth of approximately 210 MHz.

Once the two time correlation function is determined from the Heisenberg equations of motion, we need to relate it to an orthonormal set of temporal modes. To accomplish this the field operators $\hat{E}_s^{(+)}$ and $\hat{E}_s^{(-)}$ are expressed as an expansion in coherence modes,

$$\hat{E}_s^{(-)}(z,\tau)=\left[\frac{2\pi\hbar\omega_s}{c}\right]^{1/2}\sum_n \hat{a}_n^{\dagger}\psi_n(\tau) , \quad (6)$$

where $\hat{a}_n^{\dagger}$ is the creation operator for the nth mode and $\hat{E}_s^{(+)}$ is given by the Hermitian conjugate of Eq. (6). Below pump depletion the Raman equations are linear so the coherence modes evolve independently. Since the phases of the modes are statistically independent, the cross terms will drop out when Eq. (6) is inserted into Eq. (3) to relate the coherence modes to the correlation function. Defining $\lambda_n=\langle a_n^{\dagger}a_n\rangle$ the correlation function is

$$G(\tau_1,\tau_2)=\sum_n \lambda_n\psi_n(\tau_1)\psi_n(\tau_2) . \quad (7)$$

Using the orthonormality of the modes Eq. (7) can be converted to the integral equation

$$\int_{-\infty}^{+\infty} G(\tau,\tau')\psi_n(\tau')d\tau'=\lambda_n\psi_n(\tau) . \quad (8)$$

This integral is well defined for a pulsed laser because $G(\tau,\tau+\Delta)\Longrightarrow 0$ as $\Delta\Longrightarrow\infty$. To solve this integral equation for the temporal modes, $G(\tau_1,\tau_2)$ and $\psi_n(\tau)$ were converted to discrete functions of time and the integral was replaced by a sum. The resulting eigenvalue equation was then solved on an AT&T 6300 plus microcomputer using a standard routine from Argonne National Laboratory. We divided time into 89 steps and the resulting eigenvalue problem took about 3 min to solve. The solution vectors are the desired temporal modes and the corresponding eigenvalues give the average level of excitation of the mode. A list of the first 15 eigenvalues are given in Table I, and the first three modes are plotted in Fig. 1. Qualitatively the modes look very much like harmonic oscillator wave functions. In analogy with harmonic oscillator wave functions the higher-order modes are weighted more on the temporal wings. This will become important when the fields are propagated through depletion. The characteristic ratio $\Gamma\sigma/gz$ which indicates the number of significantly excited modes is also shown in Table I.

TABLE I. Statistical weights for the 15 dominant coherence modes. The value of $\Gamma\sigma/gz$ indicates the number of significantly excited modes. Brackets denote powers of ten.

$\Gamma\sigma/gz$	n	λ_n
1.9	1	0.587
	2	0.2376
	3	0.994[−1]
	4	0.428[−1]
	5	0.189[−1]
	6	0.860[−2]
	7	0.410[−2]
	8	0.191[−2]
	9	0.935[−3]
	10	0.468[−3]
	11	0.239[−3]
	12	0.125[−3]
	13	0.663[−4]
	14	0.360[−4]
	15	0.199[−4]

To generate the complex fields for a member of the ensemble, the modes are added together, each with a random phase uniformly distributed between 0 and 2π, and Gaussian weighted amplitude given by[15]

$$P(|a_n|)=2\frac{|a_n|}{\lambda_n}\exp\left[\frac{-|a_n|^2}{\lambda_n}\right] , \quad (9)$$

where a_n is a Gaussian complex random variable. To generate random amplitudes for $|a_n|$, we calculated the required mapping which turned out to be

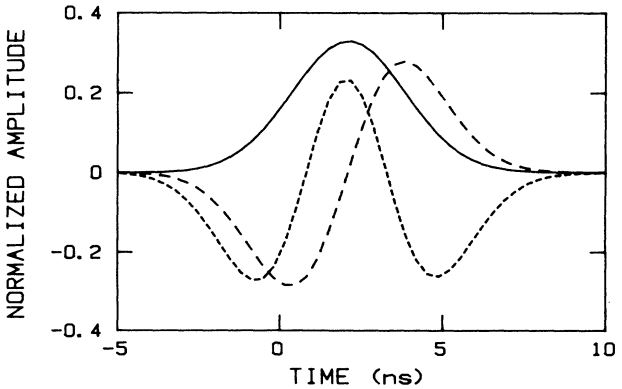

FIG. 1. First three temporal modes generated using the coherence-mode theory. The modes resemble harmonic-oscillator functions. Higher modes are weighted more on the temporal wings.

$$|a_n| = \sqrt{-\lambda_n \ln(1-x)} \ , \tag{10}$$

where x is a random number with constant probability density between 0 and 1. Thus the computer picked an x and the calculated $|a_n|$ was used as the amplitude of the nth mode. Thus at this point we have a prescription for generating an ensemble of pulses before depletion without ever converting the q-number equations to c-number equations.

B. Propagation through depletion

In order to make a comparison with our experimental data the generated ensemble of fields must be propagated through pump depletion. This was done numerically using the full nonlinear, coupled, semiclassical equations,[16]

$$\begin{aligned} \frac{\partial E_s}{\partial z} &= k_1 k_2 E_L Q^* \ , \\ \frac{\partial E_L}{\partial z} &= -k_1 k_2 E_s Q \ , \\ \frac{\partial Q^*}{\partial \tau} &= -\Gamma Q^* + E_L^* E_s \ , \end{aligned} \tag{11}$$

where now the Stokes field and system operators have been replaced by c numbers. This is valid because of the large amplitudes involved. The Q in Eq. (11) is defined in terms of the atomic matrix element Q_{RMC} in Ref. 16 (RMC stands for Raymer, Mostowski, and Carlsten),

$$Q = \frac{i}{k_1} \left[\frac{\omega_L}{\omega_s} \right]^{1/2} Q_{\mathrm{RMC}} \ . \tag{12}$$

Q_{RMC} is the c-number analog of the $\hat{Q}$ operator in Eq. (1). For completeness a Langevin driving term should be included in the equation for Q, however for large field strengths it should have no effect. Each member of the ensemble of Stokes pulses was used as a Stokes seed to produce a member of the ensemble after depletion. The ensemble average intensity of the Stokes seed was adjusted to be approximately 1% of the pump intensity. This insured that the modes had not yet begun to compete for pump photons. However at this energy the coherence modes have on the order of 10^{12} photons, justifying the use of the semiclassical equations. The same pump pulse that was used to generate the coherence modes was used as the initial E_L for the depletion program. This leaves the length of the nonlinear region as the one remaining parameter to adjust. By comparing with the experimental depleted temporal pump pulses, the gain distance was adjusted to give the observed amount of depletion or equivalently the correct Stokes pulse duration.

Both before and after pump depletion the power spectrum for each member of the ensemble was calculated using a fast Fourier transform program. Finally, using this ensemble of shots a comparison can be made with the experimental results.

III. EXPERIMENTAL RESULTS

For our experiment a frequency doubled, single-mode, Nd:YAG (YAG stands for yttrium aluminum garnet) laser operating at 532 nm was used to pump a multipass Raman cell. The 1.5-m cell was centered between two concave mirrors with a focal length of 50 cm (Fig. 2). The pump laser beam entered the multipass cell though a hole in one mirror and did not retrace its path before exiting through a hole in the opposite mirror. There are beam crossings in the multipass cell, however, they are separated by more than the laser pulse length. The beam had a confocal parameter of 38 cm and made 15 passes through the Raman cell. The laser pulse had a nearly Gaussian temporal profile with a full width at half maximum (FWHM) of 26 ns and approximately 1 mJ of energy. No anti-Stokes or second Stokes radiation was observed due dispersion and loss through the multipass cell mirrors.

The Stokes pulse grew from spontaneous emission and at the exit of the cell had fully depleted the central portion of the pump laser pulse. A typical Stokes pulse had a 2–3 ns rise and fall time and a FWHM of 12 ns. The Stokes beam was then expanded and passed through a parallel plate Fabry-Pérot interferometer with a plate spacing of 15 cm and a finesse of approximately 75. The divergence of the Stokes beam was adjusted to obtain two orders of rings. A lens at the exit of the interferometer focussed the rings onto a photodiode array which sampled a cross section of the ring pattern. The array was interfaced to a computer which then scaled the data to produce a power spectrum of the Stokes pulse. Thus our experimental setup allows us to make a power spectrum measurement on a single shot.

To monitor the frequency stability of the pump laser pulse, its power spectrum was also monitored using a second Fabry-Pérot interferometer. Thermally induced mode jumps were observed to occur approximately once in every 500 shots. In between these jumps, the laser frequency was stable to 10 MHz. Using this monitor we were able to insure that data on the Stokes pulse was taken only during periods of pump laser stability.

The experiments were done with 32 atm of H_2 in the Raman cell. At 32 atm the collisionally broadened Ra-

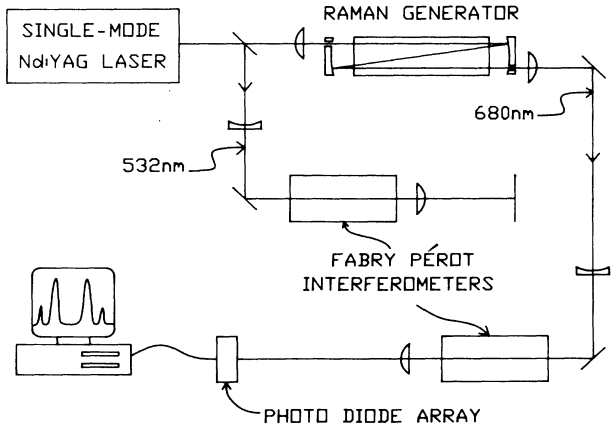

FIG. 2. Experimental setup using a multipass H_2 Raman cell and two Fabry-Pérot interferometers to monitor both pump and Stokes single-shot power spectra. The Fabry-Pérot in the pump leg was only used to detect mode hops. The pump pulse was observed to be stable to 10 MHz between mode hops.

man linewidth is 1.5 GHz FWHM.[14] Due to gain narrowing we expect that for large gain the linewidth will be reduced by a factor given by[16]

$$W_F/W_I=\sqrt{[\ln(2)/\ln(P_F/P_I)]}=\sqrt{\ln(2)/gz}\ , \quad (13)$$

where P_I and P_F are the initial and final Stokes powers and gz is the Raman gain times the length of the medium. Note that this gain narrowing factor is very insensitive to the measured final Stokes power. For example a factor of 2 uncertainty in power leads to a 1% uncertainty in the narrowing factor. Using an initial Stokes power of $P_I=\hbar w\Gamma/2$ which corresponds to one half photon per mode under the Raman linewidth (Γ), the gain narrowing factor in our experiment is predicted to be 1/6.85 resulting in a gain narrowed linewidth of 219 MHz FWHM at 32 atm. The measured power spectrum from two shots are shown in Fig. 3, along with the predicted gain narrowed linewidth. The location of the gain narrowed line was visually centered about the measured power spectrum. As can be seen from the data in Fig. 3(a), the power spectrum observed on some shots is considerably narrower than the predicted gain narrowed profile. In fact the width of the spectrum shown in Fig. 3(a) is 60 MHz (FWHM) which is close to the transform limit of the Stokes temporal pulse. A similar effect has also been observed in an infrared cavityless laser.[17] Figure 3(b) is an example of a shot which is far from transform limited. This shot must have contained significant phase or amplitude variations to generate the complex spectral structure.

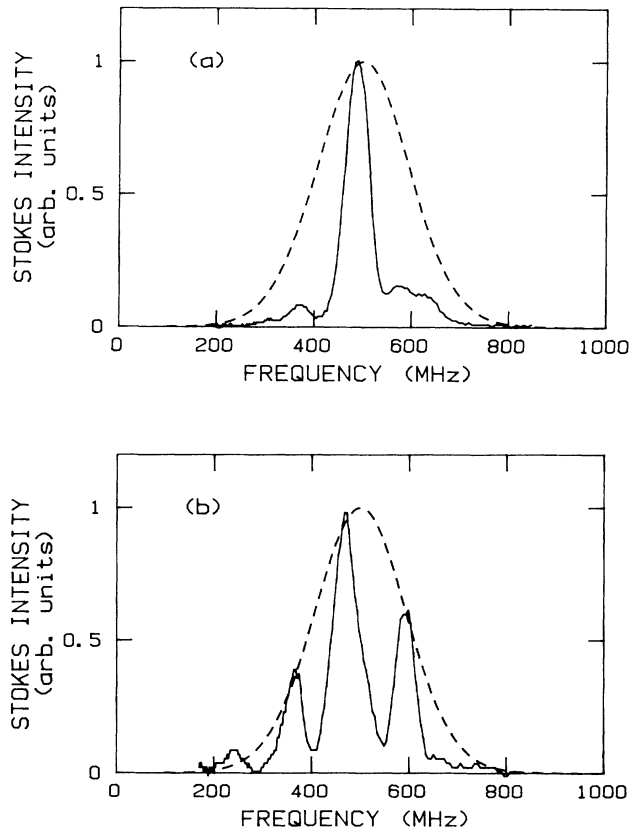

FIG. 3. (a) Experimental example of a single-shot Stokes spectrum consisting of one near transform limited spike (solid curve) which is substantially narrower than the predicted gain narrowed linewidth (dashed curve). (b) Experimental example of a single-shot Stokes spectrum with several narrow spikes (solid curve). The predicted gain narrowed linewidth (dashed curve) is shown for comparison.

For calculating statistics 44 single shot power spectra were recorded. The average spectrum obtained from these shots is shown in Fig. 4 along with the predicted gain narrowed line shape. Although the experimental curve still has some statistical variations due to the small ensemble used, the gain narrowed linewidth appears to be recovered.

In order to make a quantitative comparison with theory the two frequency spectral correlation function was calculated from the experimental data using the definition

$$C(\Delta v)=\left\langle \int_{-\infty}^{+\infty} I(v+\Delta v)I(v)dv \right\rangle , \quad (14)$$

where $I(v)$ is the single-shot energy spectrum and the brackets denote an average over the ensemble. The experimental correlation function is shown in Fig. 5 along with the correlation function generated using the coherence-mode theory.

IV. COMPARISON WITH COHERENCE-MODE THEORY

A qualitative comparison between experiment and theory can be made by comparing spectra of individual shots. For this comparison two theoretically generated spectra are shown in Fig. 6. From these examples it is clear that the theory can generate spectra similar to those produced in the experiment (Fig. 3). The gain narrowed linewidth which was recovered from the experimental average is also generated theoretically because the gain was adjusted to give the observed average linewidth.

The theoretical spectral correlation function in Fig. 5 was calculated using an ensemble with 300 members. Before comparing with experiment the theoretical curve

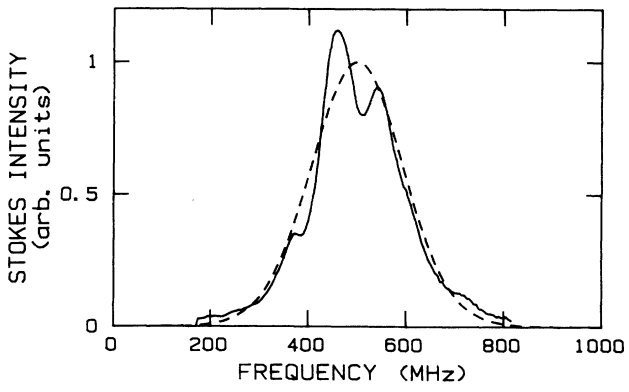

FIG. 4. Experimental power spectrum resulting from the averaging of 44 shots (solid curve). Note that this ensemble average has a width that is comparable to the predicted gain narrowed linewidth (dashed curve).

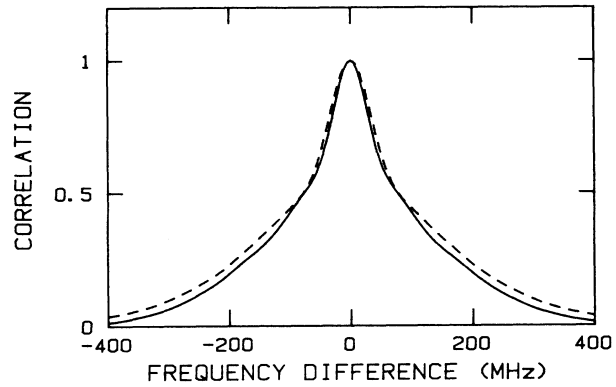

FIG. 5. Autocorrelation from experiment (solid curve) and autocorrelation calculated from the coherence-mode theory including instrument resolution (dashed curve). The small difference may be due to the small experimental ensemble used.

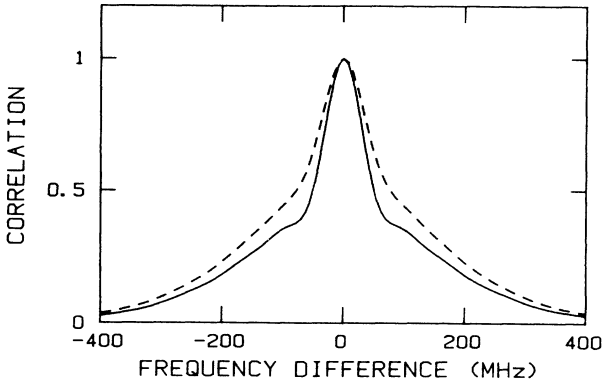

FIG. 7. Autocorrelation calculated from the coherence-mode theory with infinite instrument resolution (solid curve) and with a Fabry-Pérot resolution of 14.3 MHz (FWHM) (dashed curve). The instrument resolution obscures the shoulder which is generated in the nonlinear regime. The dashed curve is also shown in Fig. 4 for comparison with experiment.

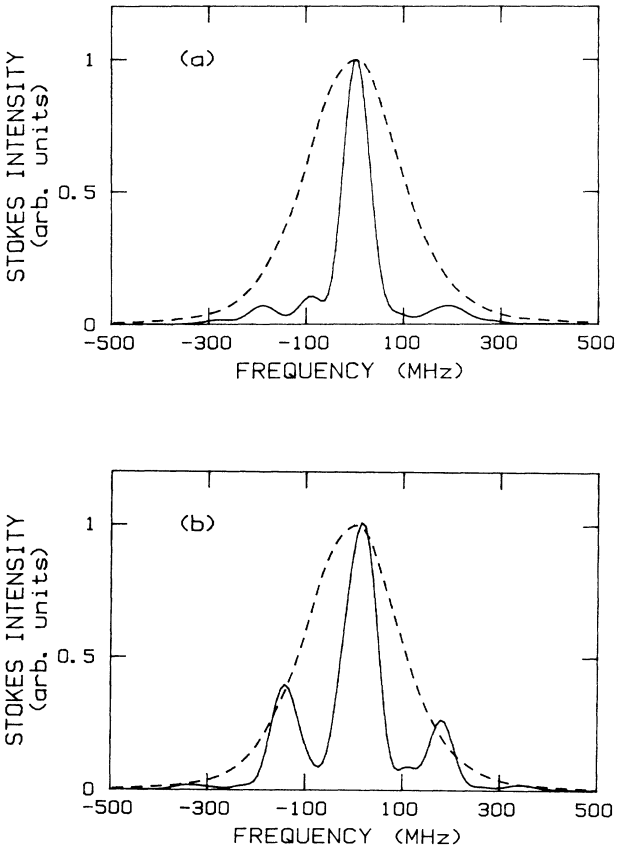

FIG. 6. (a) Theoretically generated sample of a single-shot Stokes spectra. The theory can generate near transform limited pulses similar to the experimental example of Fig. 3(a). (b) Example of a theoretically generated single shot Stokes spectra with multiple spikes similar to the experimental shot in Fig. 3(b). These examples show qualitative agreement with experiment.

was convolved with the instrument function for the Fabry-Pérot interferometer which is an Airy function. The Fabry-Pérot had a spacing of 15 cm giving a free spectral range of 1 GHz. The instrument finesse was determined by setting up the Fabry-Pérot in a similar configuration using a HeNe laser. This gave a finesse between 70 and 80 so we used 75 in our calculations which corresponds to an Airy peak with 14.3 MHz (FWHM).

The width of the central peak in the correlation function is a measure of the width of the frequency spikes in the power spectra and the background is due to the ensemble average linewidth. The theoretical correlation function before and after convolution with the Airy function are shown in Fig. 7. The effect of the finite resolution is to round out the shoulders in the correlation curve. The resolution corrected curve is plotted as the solid curve on top of the experimental data in Fig. 5. The amplitude of the theoretical and experimental curves were adjusted to one. To within the accuracy of our experiment the two curves agree.

V. DISCUSSION ON PROPAGATION THROUGH DEPLETION

At this point the theory sufficiently explains our experimental observations. In addition the theory gives some insight into how the power spectrum evolves through depletion. The coherence-mode theory cannot be used in the region where the pump beam is depleting because it assumes that the modes are independent and therefore not competing for pump energy. Thus we use the semiclassical equations which are valid because of the large field amplitudes involved. To investigate the propagation through depletion we used two sets of Stokes seed ensembles. The first set was generated from coherence modes by adding together the 15 largest statistically weighted modes. The second set was made up from the three largest modes. The set using 15 modes gives a slightly better and presumably correct result.

We first present results before and after depletion using

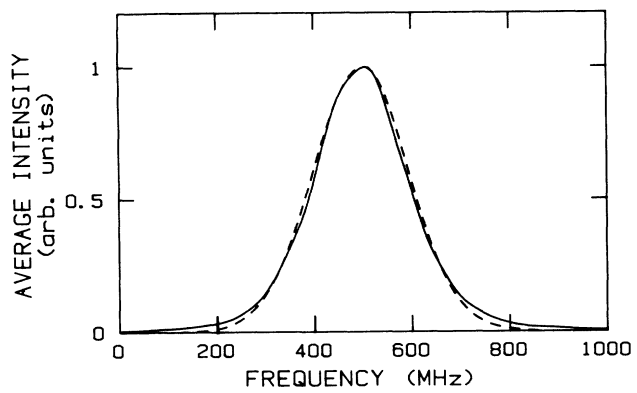

FIG. 8. Ensemble average power spectrum calculated using 15 temporal modes for 300 ensemble members before pump depletion (dashed curve) and after pump depletion (solid curve). Pump depletion leaves the average linewidth unchanged as the uncorrelated wings of the Stokes pulse are amplified.

15 modes to generate a 300-member ensemble. Figure 8 shows the results for the average linewidth. There is essentially no change in the linewidth through depletion. This is consistent with the simple gain narrowing result because after growing 13 orders of magnitude from quantum noise the last order of magnitude has little gain narrowing effect. Two examples of the Stokes temporal pulses are shown in Fig. 9 from which the spectra in Fig. 6 were calculated. Note that the temporal pulse becomes much longer through depletion, growing from roughly 5 ns before depletion (as seen from the width of the predominate mode in Fig. 1) to 12 ns after depletion. For the linewidth to remain unchanged through depletion the average time scale for fluctuations in the Stokes pulse must remain fairly constant. Since the final Stokes pulse has only minor amplitude fluctuations it must have large phase variations to maintain the linewidth.

The spectral autocorrelation functions before and after depletion are shown in Fig. 10. The autocorrelation function has two characteristic widths associated with it. The broad overall width is the result of the ensemble average line width of the pulse and the narrower central width is indicative of the frequency width of the individual peaks which make up the various spectra. The width of the individual spikes cannot be narrower than the Fourier transform of the Stokes pulse. The correlation function for a Gaussian power spectrum is $\sqrt{2}$ broader than the spectrum. The gain narrowed linewidth is very nearly Gaussian and even though the individual frequency spikes are not Gaussian we would expect that the characteristic width of their contribution to the correlation function would be approximately $\sqrt{2}$ broader than their width. Before depletion the average duration of the Stokes pulse (the average temporal Stokes pulse is given by the diagonal of the G matrix) was 4.7 ns and its Fourier transform was 95 MHz. This predicts a width of 134 MHz for the central peak in the correlation curve. We also expect the width of the background of the auto-

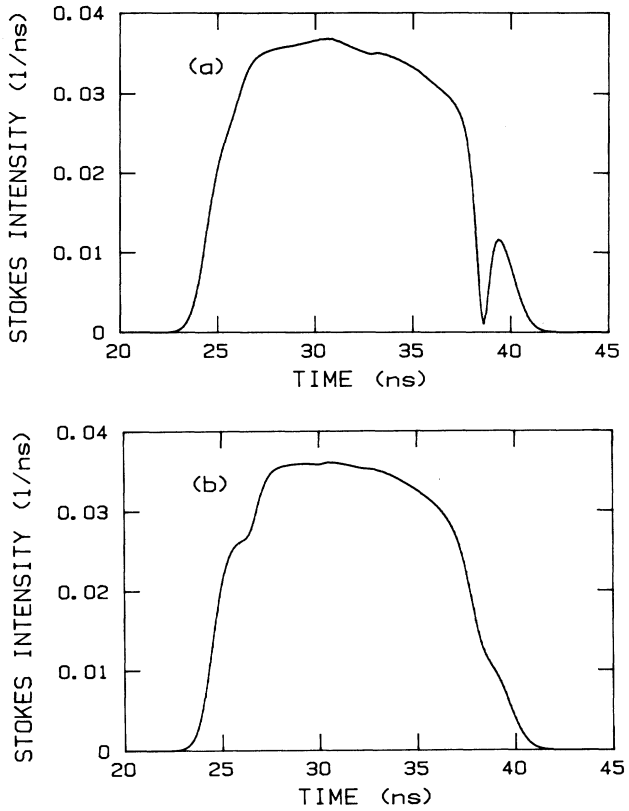

FIG. 9. (a) Theoretical temporal Stokes pulse corresponding to the spectra shown in Fig. 6(a). The pulse is fairly smooth except for the soliton pulse which is forming at the trailing edge. This particular soliton dip has little effect on the spectra because it involves only a small fraction of the pulse energy. The normalized pump intensity had a peak value of 0.0376 (1/ns) for comparison. (b) Temporal pulse corresponding to the spectra shown in Fig. 6(b). This pulse is again fairly smooth and similar to Fig. 6(a), even though its spectra is much noisier. This indicates that the average linewidth is determined by phase variations and not amplitude variations.

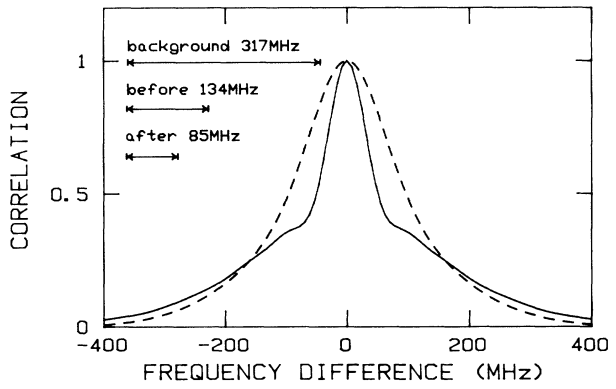

FIG. 10. Autocorrelation calculated from the coherence-mode theory before pump depletion (dashed curve) and after pump depletion (solid curve). The central portion narrows though pump depletion because the temporal Stokes pulse becomes longer. The characteristic width of the uncorrelated background and the widths of the central peak are shown before and after pump depletion.

correlation function to be $\sqrt{2}$ wider than the average line width which is 224 MHz both before and after depletion. This predicts a width of 317 MHz for the background. If two Gaussian, each with an amplitude of one half and having widths of 95 and 317 MHz, are added together the correlation curve is very nearly reproduced as shown in Fig. 11. This is reminiscent of the correlation function of continuous wave chaotic light for which the central peak is twice as high as the uncorrelated background.

After depletion the Stokes pulse is longer and its transform is 60 MHz. Multiplying by $\sqrt{2}$ gives a width of 85 MHz for the narrower of the two characteristic widths of the correlation function. The frequency widths for the central peak before (134 MHz) and after (85 MHz) depletion and that of the background (317 MHz) are marked in Fig. 10 for comparison.

The shape of the correlation function before depletion indicates that the pulse is fairly coherent and the width of the average spectra is largely due to the transform limit of the Stokes pulse which is 95 MHz. As the Stokes pulse grows through depletion the temporal wings are amplified. Fluctuations in the temporal wings are amplified thus preserving the spectral linewidth.

When generating Stokes ensembles using coherence modes theory, the higher order modes place fluctuations in the temporal wings even though their amplitude are relatively small. To demonstrate this a second ensemble was generated using only the three most excited modes. Before depletion the average linewidth was quite close to the 15-mode calculation. However after depletion the spectral wings are clearly reduced. A comparison of the linewidth after depletion using 3 and 15 modes is shown in Fig. 12. Although the higher modes have smaller statistical weights as listed in Table I they are largest in the temporal wings where the lower modes are small. As seen in Table I the average excitation of the fourth mode

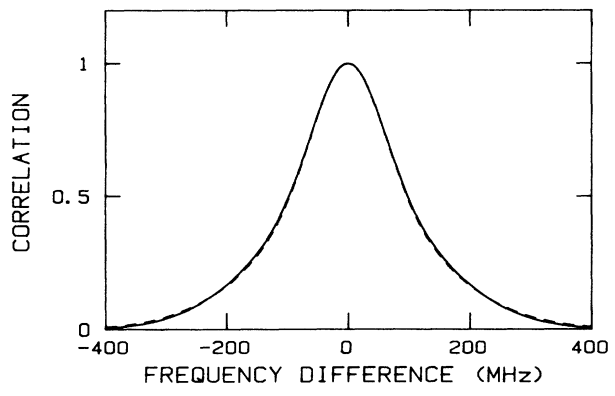

FIG. 11. Sum of two Gaussian of equal weight, one representing the correlation due to the overall background and one representing the correlation due to a transform limited pulse (solid curve), and the autocorrelation function before depletion (dashed curve). This is consistent with autocorrelation function of chaotic light for which the central peak is twice as large as the uncorrelated background.

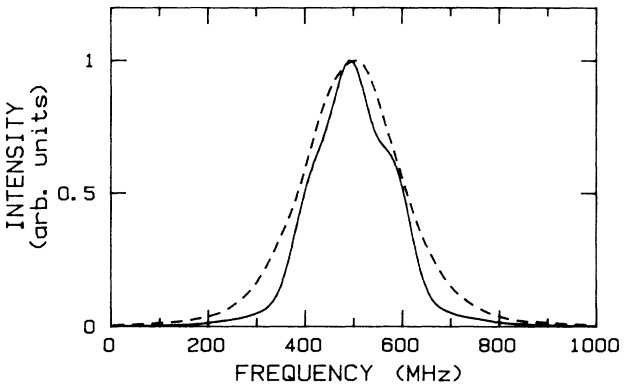

FIG. 12. Ensemble average power spectrum calculated using only three temporal modes for 300 members before pump depletion (dashed curve) and after pump depletion (solid curve). Without the weaker modes to place fluctuations in the Stokes wings, the spectrum becomes narrower through depletion.

is more than or order of magnitude smaller than that of the first mode yet it still has a significant effect on the line shape as the pulse is depleted.

In addition to spectral fluctuations some temporal Stokes pulses have a sharp dip after depletion and the pump pulse has a corresponding spike. An example can be seen in the trailing edge of the Stokes pulse shown in Fig. 9(a). This type of feature has been studied earlier[4,18,19] and has been shown to be a forming soliton. The nonlinear equations have soliton solutions in the limit of no collisional damping ($\Gamma=0$). The soliton formation is initiated by a near π phase shift in the Stokes pulse at the start of depletion. The phase shift originates in the quantum initiation. The second coherence mode has a π phase shift at $\tau=2$ ns as seen in Fig. 1. In fact all but the first mode has one or more phase shifts. However when the modes are statistically added together with random phases, the result is usually a phase drift instead of an abrupt phase shift. Nonetheless on occasional shots a sharp phase shift is generated in the linear growth region and a soliton pulse is initiated. The statistics of the pulses have been calculated[4] and measured.[18] Similar phase shifts or phase waves have been predicted to occur in superfluorescence.[8]

VI. ALTERNATE THEORETICAL APPROACHES

Although the coherence modes approach provides a convenient and somewhat intuitive way of modeling Raman generation, an alternate c-number approach can also be used. To use the c-number approach the field and atomic operators are replaced by c-number variables and the Langevin noise operator is replaced by a classical random variable.

The solution of Eq. (1) for the single transverse mode Stokes field operator as derived in Ref. 1 is

$$\hat{E}_s^{(-)}(z,\tau)=\hat{E}_s^{(-)}(0,\tau)-ik_2E_L(\tau)e^{-\Gamma\tau}\int_0^z dz'\,\hat{Q}^\dagger(z',0)I_0([4k_1k_2(z-z')p(\tau)]^{1/2})$$
$$+(k_1k_2z)^{1/2}E_L(\tau)\int_0^\tau d\tau'\,e^{-\Gamma(\tau-\tau')}E_L^*(\tau')\hat{E}_s^{(-)}(0,\tau')\frac{I_1(\{4k_1k_2z[p(\tau)-p(\tau')]\}^{1/2})}{[p(\tau)-p(\tau')]^{1/2}}$$
$$-ik_2E_L(\tau)\int_0^\tau d\tau'\int_0^z dz'\,e^{-\Gamma(\tau-\tau')}\hat{F}^\dagger(z',\tau')I_0(\{4k_1k_2(z-z')[p(\tau)-p(\tau')]\}^{1/2})\,, \tag{15}$$

where the $I_n(x)$ are modified Bessel functions and

$$p(\tau)=\int_0^\tau|E_L(\tau')|^2d\tau' \tag{16}$$

is the power of the laser field integrated up to time τ. In order to integrate the c-number analog of Eq. (15) numerically, one needs to decide what to specify for the initial conditions for $Q(z,0)$ and $E_s(0,\tau)$ and the magnitude of the Langevin fluctuations. The choice will depend on whether in the final result one calculates normal ordered quantities or antinormal ordered quantities. Since detectors measure intensity which is a normal ordered quantity, one should use normal force. The ordering is important when calculating low level intensities where a difference of one photon is significant. However at the end of the Raman generator the fields are quite large and thus classical so that the difference between the two orderings is expected to be extremely small. For normal ordering one can use the square root of $\langle Q^\dagger(z,0)Q(z,0)\rangle$, $\langle a^\dagger(0,\tau)a(0,\tau)\rangle$, and $\langle F^\dagger(z,\tau)F(z,\tau)\rangle$ to determine the magnitude of the fluctuations. The reverse operator ordering is used for the antinormal ordered approach.

When using normal ordering there is no contribution from the vacuum field but there are contributions from $Q(z,0)$ and $F(z,\tau)$. $\langle Q^\dagger(z,0)Q(z,0)\rangle$ is the initial linear number density. However for times large compared to $1/\Gamma$ the contribution from the initial Q decays as can be seen from Eq. (15). This is unphysical because one would expect that an initial polarization fluctuation in the medium would be amplified as the laser pulse passes and lead to a substantial Stokes field for most of the pulse duration. This problem arises because of the way we have phenomenologically included damping. To maintain consistency the Langevin term is added. To calculate the expectation value $\langle F^\dagger(z,\tau)F(z,\tau)\rangle$ the second of Eqs. (1) is used with the laser driving field omitted. $\langle F^\dagger(z,\tau)F(z,\tau)\rangle$ is found to be proportional to the linear number density of the atoms in the ground state minus the linear density of the atoms in the excited state $|3\rangle$ which is essentially the linear number density in the ground state. This "large" Langevin force generates a contribution in the last term of Eq. (15) which properly accounts for the initial polarization fluctuations plus the polarization fluctuations occurring after $\tau=0$.

On the other hand if one choose to use antinormal ordering there is no contribution from $\langle Q(z,0)Q^\dagger(z,0)\rangle$ but now there is a contribution from the vacuum field. In addition, the expectation value from the Langevin force, $\langle F(z,\tau)F^\dagger(z,\tau)\rangle$, is now "small" and proportional to the linear density of atoms in the excited state $|3\rangle$. This Langevin force preserves the number of atoms in state $|3\rangle$ in the absence of driving fields. Since the fraction of atoms in state $|3\rangle$ is quite small one would expect that the contribution from the Langevin term would also be small.

When performing a c-number calculation, it is advantageous to use antinormal ordering because as we will show the Langevin term can in fact be neglected. This also has been verified by Englund.[19] Omitting the Langevin term greatly decreases the computing time because this term contains a double integral. To show that the Langevin term can be omitted when using the antinormal ordered approach to calculate large-field amplitudes, we performed the c-number calculation without the Langevin force and then compared the results with those obtained from the normal-ordered coherence-mode theory.

We initiate the Stokes field by including random noise in the initial Stokes field. Since the final Stokes field is much larger than the initiating noise the first term in Eq. (15) can be ignored leaving only the third term. To generate an ensemble member the operators were replaced with c-number variables. As with the coherence modes approach this equation is only valid in the linear regime before pump depletion. Therefore the resulting field from the c-number analog of Eq. (15) was used as the Stokes seed in the semiclassical nonlinear equations for propagation through depletion.

Our input vacuum noise field was created by summing up a set of sine wave modes with random phases. The vacuum field should contain all frequencies; however only those near resonance will experience gain. The frequency spacing of the noise modes was chosen by the resolution of the system. Experimentally, our pump beam was approximately Gaussian with a FWHM of 26 ns. Taking the Fourier transform produced a frequency spectrum with a $1/e$ width of 20 MHz. Thus a 20-MHz spacing of the modes resulted in a finer spacing than the resolution of the system, making for an effective zero spacing. By using 159 modes centered about the Raman resonance, the initiating Stokes noise covered approximately twice the Raman linewidth.

Starting with this noisy input field, we evaluated the Stokes field with the same gain that was used in the coherence modes approach. With this gain the Stokes noise grew by 12 orders of magnitude. This is consistent with starting with $\hbar\omega/2$ in each optical mode, weighted by the Lorentzian Raman linewidth, and then amplifying to 0.01 mJ pulse energy. As in the coherence-mode approach the final two orders of magnitude of amplification through depletion were done using the nonlinear stimulated Raman scattering (SRS) equations.

The final linewidth and spectral correlation function generated using this approach were essentially identical with those calculated using coherence modes. A compar-

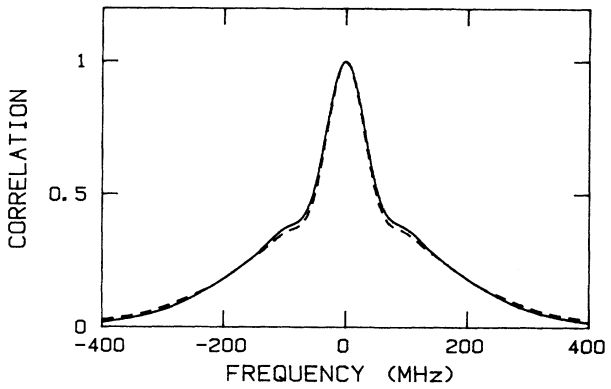

FIG. 13. Comparison of the correlation function calculated using coherence mode theory (dashed curve) and using semiclassical theory with random Stokes noise (solid curve). The two methods give essentially the same results despite the lack of a Langevin noise term in the semiclassical approach.

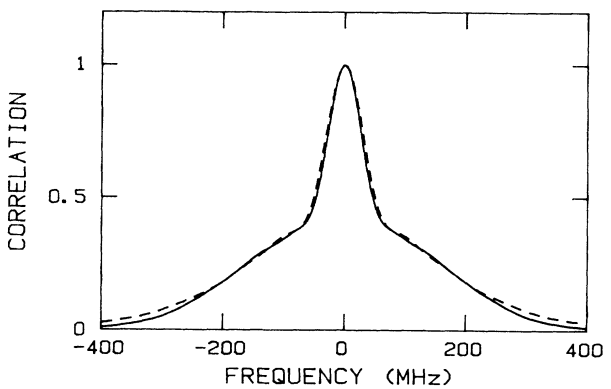

FIG. 14. Comparison of the autocorrelation function between coherence-mode theory (dashed curve) and that calculated using the gain narrowed noise approach. The close agreement suggests that the details of the Stokes initiation and growth through the linear regime have little effect on the final statistics.

ison of the correlation functions are shown in Fig. 13. Also the single-shot spectra showed similar fluctuations, with many of the narrower peaks approaching the transform limit. Comparing this approach with the more exact theory of the coherence-mode representation, we found that the two theories gave essentially identical results, despite the lack of any Langevin contributions in the c-number calculation. We expect this is true because the collisional noise just rerandomizes the initiating quantum noise. Thus this experiment cannot determine the effect of the collisional noise on an individual shot. The lack of dependence of the statistics on the Langevin noise term is somewhat unfortunate because this experiment cannot test the validity of the Langevin approach.

As a third and simpler approach we generated large amplitude noise to use as a seed for propagation through depletion. This noise was generated by again adding together closely spaced sine waves but weighted by the gain narrowed linewidth instead of the full Raman linewidth. This eliminated the linear growth region and started the calculation at the onset of pump depletion. The average temporal profile of the Stokes seed was assumed to be the same as that produced using the c-number equations before depletion. For this reason the c-number equations had to be integrated first; however, information about the individual fluctuations is not carried over from the c-number calculation. We called this the gain narrowed noise approach.

Using the gain narrowed noise as the Stokes seed we again obtained the large spectral fluctuations after depletion. The resulting spectral correlation function shown in Fig. 14 was also very similar to that obtained using the coherence-mode approach and thus in agreement with experiment.

From the gain narrowed calculation we conclude that the observed spectral fluctuations are a result of amplifying a random temporal segment of chaotic light. These fluctuations tell us little about the fluctuations added to the pulse by collisions as the pulse is amplified. However, it may be possible to see the effects of collisional noise if the output from a Raman generator is split and then amplified in two separate amplifiers. A correlation in the spectra from the two amplifiers should be affected by the different collisional noise which is added in the two amplifiers.

ACKNOWLEDGMENTS

We would like to thank M. G. Raymer for helpful discussions on the coherence-mode theory and J. C. Englund and C. M. Bowden for insightful discussions on quantum initiation. This research was supported by the National Science Foundation under Grant No. PHY-8516110.

[1]M. G. Raymer and J. Mostowski, Phys. Rev. A **24**, 1980 (1981).
[2]I. A. Walmsley and M. G. Raymer, Phys. Rev. A **33**, 382 (1986); N. Fabricius, K. Nattermann, and D. von der Linde, Phys. Rev. Lett. **52**, 113 (1984).
[3]D. C. MacPherson, R. C. Swanson, and J. L. Carlsten, Phys. Rev. Lett. **61**, 66 (1988).
[4]C. M. Bowden and J. C. Englund, Opt. Commun. **67**, 71 (1988).
[5]J. C. Englund and C. M. Bowden, Phys. Rev. Lett. **57**, 2261 (1986).
[6]C. Radzewicz, Z. W. Li, and M. G. Raymer, Phys. Rev. A **37**, 2039 (1988).
[7]D. Polder, M. F. H. Schuurmans, and Q. H. F. Vrehen, Phys. Rev. A **19**, 1192 (1978).
[8]F. A. Hopf, Phys. Rev. A **20**, 2064 (1979).
[9]M. G. Raymer, I. A. Walmsley, J. Mostowski, and B. Sobolewska, Phys. Rev. A **32**, 332 (1985).

[10]M. Born and E. Wolf, *Principals of Optics* (Pergamon, New York, 1975), Secs. 10.3 and 10.4
[11]M. Lax, Phys. Rev. **145**, 110 (1965); W. Louisell, *Quantum Statistical Properties of Radiation* (Wiley, New York, 1973); H. Haken, *Laser Theory* (Springer, New York, 1983).
[12]P. W. Milonni, J. R. Ackerhalt, and W. A. Smith, Phys. Rev. Lett. **31**, 958 (1973).
[13]I. R. Senitsky, Phys. Rev. Lett. **31**, 955 (1973).
[14]W. K. Bischel and M. J. Dyer, Phys. Rev. A **33**, 3113 (1986).
[15]F. Haake, H. King, G. Schroder, J. Haus, and R. Glauber, Phys. Rev. A **20**, 2047 (1979).
[16]M. G. Raymer, J. Mostowski, and J. L. Carlsten, Phys. Rev. A **19**, 2304 (1979).
[17]S. G. Evangelides, J. R., L. Carson, B. G. Danly, and R. J. Temkin, IEEE J. Quantum Electron. **24**, 99 (1988).
[18]D. C. MacPherson, R. C. Swanson, and J. L. Carlsten (unpublished).
[19]J. C. Englund, U.S. Army Research Office Report No. TCN-87-083, 1988 (unpublished).